RSC Advances

ROYAL SOCIETY OF CHEMISTRY

www.rsc.org/advances

RSC Advances

ARTICLE

Synthesis, crystal structure and biological properties of a bismuth(III) Schiff-base complex

Chuan-Hua Li,[a] Jian-Hong Jiang,[a] Xu Li,[a] Li-Ming Tao,[a] Sheng-Xiong Xiao,[a] Hui-Wen Gu,[b] Hui Zhang,[a] Chao Jiang,[a] Jin-Qi Xie,[a] Meng-Na Peng,[a] Lan-Lan Pan,[a] Xian-Ming Xia[a] and Qiang-Guo Li*[a]

Received 00th January 2015,
Accepted 00th January 2015

DOI: 10.1039/x0xx00000x

www.rsc.org/

In this paper, a new bismuth(III) Schiff-base complex $[Bi_9O_8(vanen)_3\ (NO_3)_2\ (CH_3OH)_2\ (H_2O)]\cdot 3NO_3\cdot 5.5H_2O$ was synthesized by reaction of [H_2*vanen* =*N*, *N*′–ethylene bis(3–methoxysalicylideneimine)] and $Bi(NO_3)_3\cdot 5H_2O$ in methanol at 45~60 °C. The inhibitory effects of the complex and its ligand on *Schizosaccharomyces pombe* (*S. pombe*) growth were investigated by microcalorimetry. The experimental results indicated the complex had a stronger inhibitory activity towards *S. pombe* than that of the ligand. The interaction between bovine serum albumin (BSA) and the complex under physiological conditions was studied by fluorescence spectroscopy. The complex had a quite strong ability to quench the fluorescence of BSA and their combination reactions were a static quenching process. The complex could bind BSA via a binding site and the binding distance *r* was 3.52 nm. The synchronous fluorescence spectroscopy further revealed that the complex had partly inserted into the hydrophobic pocket of BSA.

1. Introduction

The chemistry of metal complexes with Schiff bases has drawn much attention, mainly due to their preparative accessibility, structural variability, and diverse range of applications such as catalysis, magnetism and pharmacology.[1-3] Among Schiff-base ligands, "salen-types", which are formed by the condensation of various diamines and salicylaldehyde derivatives, are perhaps the most popular ones. As typical Salen-like ligand, hexadentate Schiff base, which is famous for the possession of the N_2O_2 and O_2O_2 cavities, is usually used as the endogenous bridging units to coordinate to 3d, 4f, s, and p block metal ions and provide di/tri/oligonuclear systems.[4,5] Up to now, many coordination compounds of hexadentate Schiff base containing 3d and 4f block metal ions have been studied, while the main group elements, especially bismuth(III) complexes, are still less investigated.[6] One reason may be that single crystals suitable for the X-ray diffraction study of these compounds have been difficult to obtain. Bismuth compounds, owing to their high effectiveness and low toxicity, have long been applied in the treatment of diverse microbial infections, including syphilis, diarrhoea, gastritis and colitis.[7,8] In combination with antibiotics, basic bismuth salicylate (BSS), together with colloidal bismuth subcitrate (CBS), and ranitidine bismuth citrate, have been recommended as a standard treatment for ulcers and *Helicobacter pylori* (*H. pylori*) infection in many countries.[9] Even more important is that ^{212}Bi and ^{213}Bi compounds have been used as targeted radio-therapeutic agents for cancer treatment, and furthermore they can effectively reduce the side effects of cisplatin (*cis*-DDP) in carcinoma therapy.[10,11] Bismuth compounds display good antimicrobial and antitumour activities,[12-15] which indicates that there is a scope for the development of new and effective bismuth-based drugs.

Biological microcalorimetry, providing a quantitative and continuous measurement of heat production, can be applied to directly determine the biological activities of a living system. Heat flux is an expression of overall metabolic flux, and the detection of small changes in heat production to respond to toxic insult will be a sensitive indicator of altered metabolism. Any substances that could modify cellular metabolism, would change the power–time curve obtained from the microcalorimeter and the heat-output curves, not only thermodynamics data but also kinetic data could be derived.[16,17] Many studies have demonstrated that the test results by microcalorimetry are in agreement with that of traditional assay methods such as the agar cup method , the paper disk diffusion assay, the cylinder diffusion method, and the broth microdilution method.[18,19] Due to its good sensitivity, accuracy, and reproducibility, microcalorimetry was gradually accepted by more and more researchers, and was widely used in new drug discovery.[20]

[a] Hunan Provincial Key Laboratory of Xiangnan Rare-Precious Metals Compounds and Applications, Department of Chemistry and Life Science, Xiangnan University, Chenzhou 423000, Hunan Province, PR China. E-mail: liqiangguo@163.com
[b] State Key Laboratory of Chemo/Biosensing and Chemometrics, College of Chemistry and Chemical Engineering, Hunan University, Changsha 410082, Hunan Province, PR China.

Studies on the interaction between metal complexes and the most abundant carrier proteins (serum albumins) are an interesting topic because metal complexes for their binding properties have become suitable candidates as antimicrobial and antitumor drugs, the most important examples are cisplatin, carboplatin, and oxaliplatin.[21-23] Serum albumin has multiple binding sites and is able to interact with drug molecules and form a stable protein–drug complex which could affect the absorption, distribution, activity and toxicity of drugs.[24] Among the serum albumins, BSA is an attractive macromolecule frequently used in biophysical and biochemical studies because of its structural homology with human serum albumin (HSA), its availability, low cost and unusual ligand binding properties. The BSA molecule is composed of three domains (I, II, and III) and each domain contains two sub domains (A and B). Intrinsic fluorescence of BSA originates from two tryptophan residues possessing Trp-134 and Trp-212[25,26]

In this study, on the basis of our previous work,[27-30] we have prepared a new polynuclear oxido-cluster structure of bismuth complex derived from H_2*vanen* and bismuth nitrate pentahydrate. Then *S. pombe* was chosen as an ideal model to assess the biological activity of the complex by microcalorimetry.[31] The quenching of the intrinsic tryptophan fluorescence of BSA was used as a tool to study the interaction of the complex with this transport protein in an attempt to characterize the chemical associations taking place. As a basic research, the aim of this paper is to provide some valuable information for further study of bismuth compounds.

2. Results and discussion

2.1 Description of the structure of the complex

The complex $[Bi_9O_8(vanen)_3(NO_3)_2(CH_3OH)_2(H_2O)]\cdot 3NO_3\cdot 5.5H_2O$ crystallizes in a triclinic crystal system with space group *P*–1. Each ligand is attached to bismuth(III) ions through two imino nitrogen atoms, two phenolic oxygen atoms and two methoxyl oxygen atoms (as shown in Fig. 1a). The nine bismuth atoms and eight oxygen atoms consists of the shrouding of the Bi_9O_8 core, which can be described as a monocapped square anti-prism,[32] with Bi1/ Bi2/ Bi3/ Bi4 forming one square face and Bi5/ Bi6/ Bi7/ Bi8 constructing the other one (Fig. 1b). The dihedral angle between the two mean planes is 0.348(2)°. Atom Bi9 projects through the second of these faces to provide the cap. The coordination number of bismuth atoms is seven and the coordination modes of bismuth atoms have been divided into two different types. One is a bismuth atom linked by seven oxygen atoms, the other is a bismuth atom bonded to two nitrogen atoms except for five oxygen atoms (Fig. 1c). Partially selected bond lengths for the complex are listed in Table S1 (ESI†). The eighteen Bi–O bonds involve the deprotonated phenol oxygen atoms (from 2.396(7) to 2.842(1) Å). The six Bi–O (methoxyl) distances cover a narrow range, 2.758(1)–2.815(7) Å. The six Bi–N distances are in the range of 2.401(1) and 2.540(1) Å. The range of twenty-four Bi–O_{core} is 2.072(9) to 2.285(8) Å.

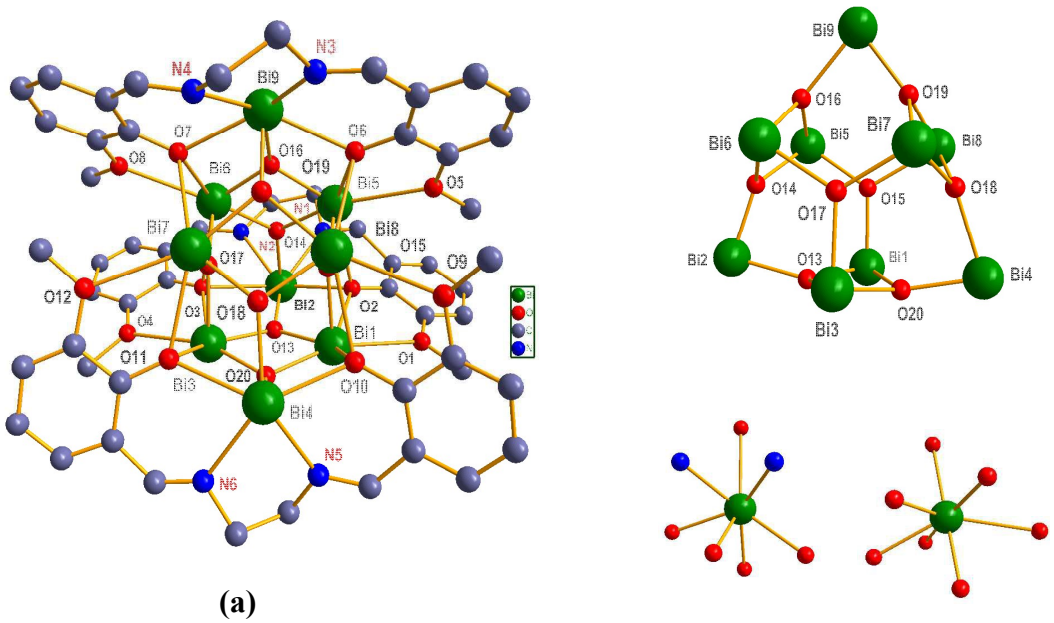

Fig. 1 (a) Crystal structure of the complex. For clarity, partial atoms are omitted and the carbon atoms of the ligands are unlabelled. (b) Perspective view of the Bi_9O_8 core. (c) The coordination modes of bismuth atoms.

2.2 Determination of inhibitory activity of the complex and its ligand on *S. pombe* growth

2.2.1 The growth rate constant (*k*) of *S. pombe* with and without drugs. Microcalorimetry was applied to evaluate the effect of the complex and its ligand on *S. pombe* growth. The inhibitory activity was recorded as power–time curves through an ampoule method with a TAM Air Isothermal Microcalorimeter. Fig. 2d shows the power–time curve of *S. pombe* without drug at 32.00 °C. Since *S. pombe* metabolic process was monitored in isothermal and isochoric conditions, oxygen and nutrient consumed by cells were supplied limitedly. The growth curve of *S. pombe* could be divided into four phases, *i.e.* a lag phase (AB), a log (exponential) phase (BC), a stationary phase (CD) and a decline phase (DE). During the log phase, the power–time curves obey the following equation[33]:

$$n_t = n_0 \exp[k(t - t_0)] \quad (1)$$

where t is the time after the start of exponential growth phase and t_0 is the start time of exponential growth phase; n_t and n_0 are the cell number at time t and t_0, respectively. If the power output of each *S. pombe* cell was one w, then

$$n_t w = w n_0 \exp[k(t - t_0)] \quad (2)$$

If $P_t = n_t w$; $P_0 = n_0 w$, then

$$P_t = P_0 \exp[k(t - t_0)] \quad (3)$$

or

$$\ln P_t = \ln P_0 + kt - kt_0 \quad (4)$$

where P_0 and P_t stand for the heat–output power at the beginning of baseline and at time t, respectively; k is the growth rate constant of *S. pombe* at specified condition, whose size represents growth speed. The thermogenic curves of the exponential phase of growth corresponds to Eq. (4), while the growth rate constant k can be obtained by fitting $\ln P_t$ and t to a linear equation. As shown in Table 2, the growth rate constant k of *S. pombe* at the different concentrations of the drugs was calculated. All correlation coefficients were greater than 0.9955, indicating a good reproducibility and correlationship. From Fig. 2 and Table 2, it could be seen that the peak time of maximum heat-output power t_p prolonged and the growth rate constant k decreased with the increase of concentration of the drugs. This is mainly because after addition of the drug into the *S. pombe* suspension, some cells were inhibited or killed, but the survivors continue to metabolize which maintain a lower level of the heat production rate, and this level is directly depending on the drug concentration.

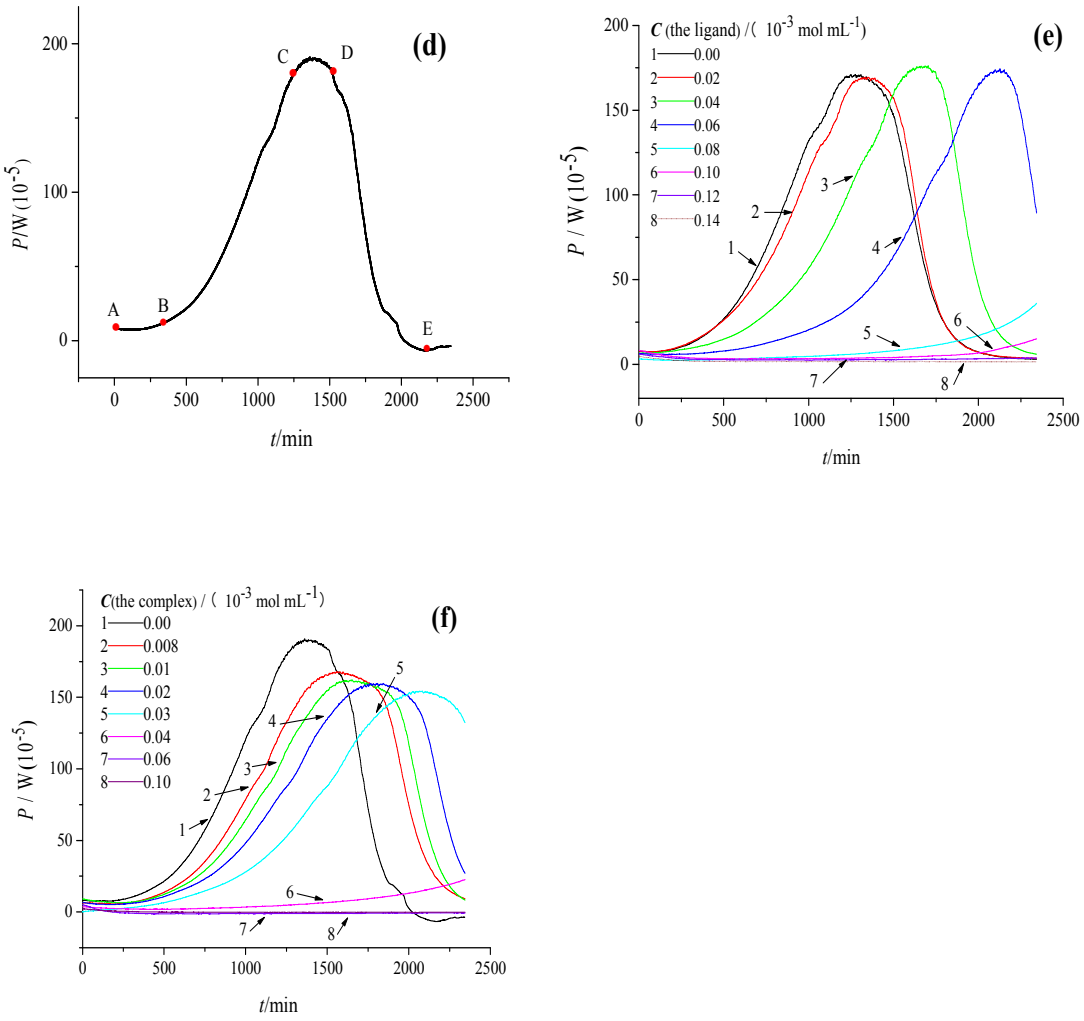

Fig. 2 Metabolism thermogenic curves of *S. pombe* cells affected by the tested drugs at 32.00 °C. (d) for control. (e) the ligand. (f) the complex.

Table 2 Thermokinetic parameters of *S. pombe* growth affected by inhibitors at different concentrations

Inhibitors	C^a/(10^{-3} mol L^{-1})	K^b /min^{-1}	R^c	I^d	IC^e_{50}/ mol L^{-1}
the ligand	0.00	0.0035 ± 4.4212 × 10^{-6} [f]	0.9976	0	
	0.02	0.0030 ± 4.7054 × 10^{-6}	0.9957	14.3	
	0.04	0.0025 ± 1.8940 × 10^{-6}	0.9988	28.6	
	0.06	0.0021 ± 1.6927 × 10^{-6}	0.9985	40.0	

	0.08	0.0012 ± 2.1767 × 10^{-6}	0.9958	65.7	
	0.10	0.0023 ± 3.9926 × 10^{-6}	0.9977	34.3	**6.7 × 10^{-3}**
	0.12	0.00002 ± 2.9650 × 10^{-6}	–0.0977	94.3	
	0.14	–	–	–	
the complex	0.00	0.0036 ± 2.9289 × 10^{-6}	0.9982	0	
	0.008	0.0034 ± 3.2407 × 10^{-6}	0.9971	5.6	
	0.01	0.0030 ± 3.3155 × 10^{-6}	0.9959	17.6	
	0.02	0.0027 ± 2.5502 × 10^{-6}	0.9967	25	**3.7 × 10^{-3}**
	0.03	0.0029 ± 3.7249 × 10^{-6}	0.9960	19.4	
	0.04	0.0013 ± 4.4363 × 10^{-6}	0.9955	63.9	
	0.06	–	–	–	
	0.10	–	–	–	

[a] The concentration. [b] the growth rate constant of *S. pombe*. [c] The correlation coefficient. [d] The inhibitive ratio.
[e] The half inhibition concentration. [f] Mean ± S.D.; n = 3.

2.2.2 The inhibition ratio (*I*) of *S. pombe*. The inhibition ratio of the growth metabolism of *S. pombe* treated by drug is defined as Eq. (5):

$$I = \frac{(k_0 - k_c)}{k_0} \times 100\% \qquad (5)$$

where k_0 is the control rate constant (without any drug inhibition) of *S. pombe* and k_c is the growth rate constant of *S. pombe* treated by an inhibitor with a concentration of *c*. IC_{50} means that when the inhibition ratio is 50%, the drug concentration is the half inhibition concentration, which can be regarded as the inhibiting concentration to cause a 50% decrease of the *S. pombe* growth rate constant. To demonstrate the inhibitory effect of the tested drugs on *S. pombe*, the values of *I* were also shown in Table 2. Then IC_{50} was calculated to be 6.7×10^{-3} mol L^{-1} for the ligand and 3.7×10^{-3} mol L^{-1} for the complex, respectively. Considering the values of growth rate constant and half-inhibitory ratio, it could be easily concluded that the complex has a stronger inhibition effect than that of the ligand on *S. pombe* growth. Thus, the sequence of inhibitory activity of the tested drugs was the complex > the ligand.

2.3 The interaction between BSA and the complex

2.3.1 The fluorescence quenching mechanism of BSA by the complex. Fluorescence quenching refers to any process, which can decrease the fluorescence intensity of a sample such as excited state reactions, energy transfers, ground-state complexes formation and collisional process.[34] The different mechanisms of quenching are usually classified as either dynamic quenching or static quenching. Dynamic and static quenching can be distinguished by their differing dependence on temperature and viscosity. Since higher temperature results in larger diffusion coefficients, the dynamic quenching constants are expected to increase with increasing temperature. In contrast, increased temperature is likely to result in decreased stability of complexes, and thus lower values of the static quenching constants. BSA has three types of intrinsic fluorophores such as tryptophan, tyrosine and phenylalanine. As Sulkowska said,[35] the intrinsic fluorescence of BSA is almost contributed by tryptophan alone because phenylalanine has a very low quantum yield and the fluorescence of tyrosine is almost totally quenched if it is ionized, or near an amino group, a carboxyl group. Here, the complex was used as a quencher to investigate the fluorescence intensity of BSA at different concentrations of the complex under physiological conditions. As shown in Fig. 3, the fluorescence intensity of BSA decreased regularly with increasing the complex concentration. BSA has a strong fluorescence emission band at 340 nm by fixing the excitation wavelength at 280 nm and the emission maximum undergoes a slight blue shift, which is mainly contributed by the tryptophan in BSA.

To confirm the fluorescence quenching mechanism of BSA by the complex, we firstly assumed that the interaction proceeded via a dynamic way. In general, quantitative analysis of the quenching phenomenon is performed via applying the Stern–Volmer equation to the fluorescence quenching data[36]:

$$\frac{F_0}{F} = 1 + K_{SV}[Q] = 1 + k_q \tau_0 [Q] \qquad (6)$$

where F_0 and F are the fluorescence intensities before and after addition of the quencher, respectively; K_{SV} is the Stern–Volmer quenching constant and $[Q]$ is the quencher concentration; K_q is the bimolecular quenching rate constant and τ_0 is the lifetime of the fluorophore in the absence of quencher. Fig. 4 displays the Stern–Volmer plots of the quenching of BSA tryptophan residues fluorescence by the complex at different temperatures. The Stern–Volmer quenching constant (K_{SV}) is inversely correlated with temperature, which indicates that the probable quenching mechanism is not induced by dynamic collision but from compound formation.[36] As the τ_0 of biomolecule was about 10^{-8} s,[37] the quenching rate constant k_q could be calculated ($K_{SV} = K_q\tau_0$). As shown in Table 3, the quenching rate constant k_q was far above the limiting diffusion rate constant (2.0×10^{10} L mol^{-1} s^{-1}).[38] These facts showed that the fluorescence quenching of BSA by the complex was a static quenching process.

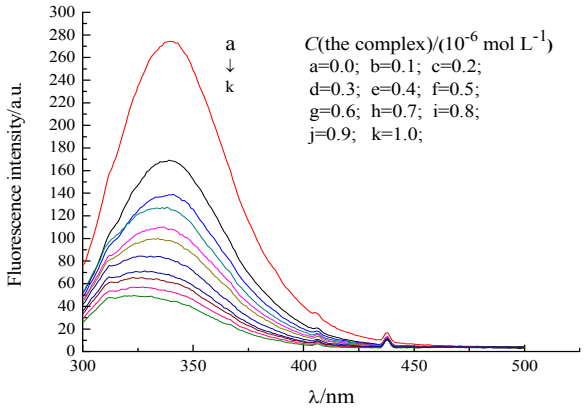

Fig. 3 The quenching effect of the complex on BSA fluorescence intensity at 298.15 K. $\lambda_{ex}/\lambda_{em}$=280nm/340 nm; c(BSA)=1.0×10^{-6} mol L^{-1}.

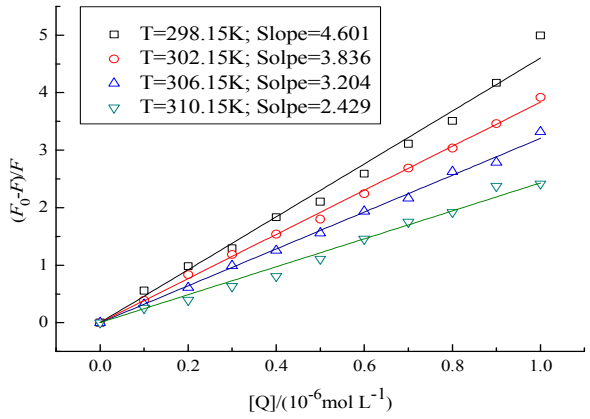

Fig. 4 The Stem-Volmer plots for the fluorescence quenching of BSA by the complex at different temperatures.

Table 3 Binding constants and number of binding sites of the system of the complex and BSA

Temperature (K)	K_q/(L mol^{-1} s^{-1})[a]	K_A/(L mol^{-1})[b]	n[c]
298.15	4.60×10^{14}	1.55×10^6	0.9249
302.15	3.84×10^{14}	2.86×10^6	0.9798
306.15	3.20×10^{14}	3.25×10^6	1.0014
310.15	2.43×10^{14}	4.77×10^6	1.0497

[a] Quenching rate constant. [b] Binding constants. [c] binding sites.

2.3.2 Binding constant (K_A) and number of binding sites (n) of BSA with the complex. When small molecules bind independently a set of equivalent sites on a macromolecule, the equilibrium between free and bound molecules is given by the equation[39]:

$$\log\left[\frac{F_0-F}{F}\right]=\log K_A+n\log[Q] \qquad (7)$$

In this equation, K_A is the binding constant and n is the number of binding sites per BSA. According to Eq. (7), one drawing was made with log[(F_0-F)/F] as ordinate and log[Q] as abscissas (see Fig. 5). The binding constants K_A and the number of binding sites n were obtained according to the Eq. (7) and Fig. 5. The binding constants (K_A) between BSA and the complex were 1.55×10^6 (298.15K), 2.86×10^6 (302.15K), 3.25×10^6 (306.15K) and 4.77×10^6 (310.15K), and the binding sites values (n) were (0.989 ± 0.05) ≈ 1 (see in Table 3). The results suggested that there was a strong binding force between BSA and the complex, and a binding site could be formed

2.3.3 Energy transfer and binding distance between BSA and the complex. According to the Förster theory, the energy transfer efficiency between the donor and the acceptor is described as the following equation[40]:

$$E=1-\frac{F}{F_0}=\frac{R_0^6}{R_0^6+r^6} \qquad (8)$$

In Eq. (8), E denotes the efficiency of transfer between the donor and the acceptor, and R_0 is the critical distance when the energy transfer efficiency is 50%; r is the binding distance between the donor and the acceptor.

$$R_0^6=8.79\times10^{-25}K^2n^{-4}\phi J \qquad (9)$$

In this equation, K^2 is the orientation factor, and Φ is the fluorescence quantum yield of donor in the absence of acceptor; n is the refractive index of the medium; J is the integral and is defined the amount of overlap between the emission spectrum of the donor and the absorption spectrum of the acceptor (Fig. 6), which can be calculated by the equation:

$$J=\frac{\int_0^\infty F(\lambda)\varepsilon(\lambda)\lambda^4 d\lambda}{\int_0^\infty F(\lambda)d\lambda} \qquad (10)$$

where F(λ) is the corrected fluorescence intensity of the donor in the wavelength range from λ to λ + Δλ; ε(λ) is the extinction coefficient of the acceptor at λ. In the present case, the following parameters were applied to these data: the space factor of orientation

K^2=2/3, the fluorescence quantum yield Φ=0.15 and the refractive index n=1.36.[41] Based on the Eqs. (8)–(10), J =3.63×10^{-13} cm^3 L mol^{-1}, R_0= 4.59 nm, E = 0.83 and r = 3.52 nm can be calculated. The binding distance r on the 2–8 nm scale,[42,43] and $0.5R_0 < r < 1.5R_0$,[44] which indicates that the energy transfer from BSA to the complex occurs with high probability.

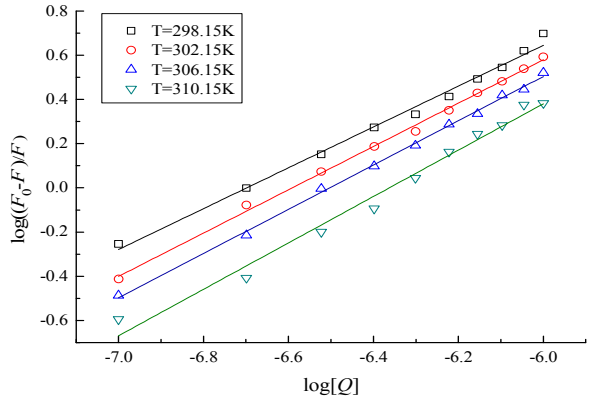

Fig. 5 Double-log plot of the complex quenching effect on BSA fluorescence at different temperatures.

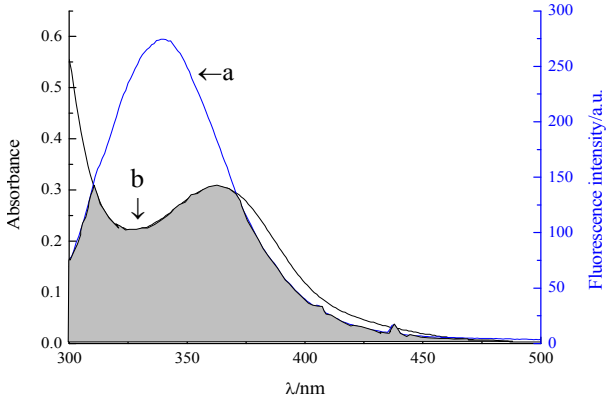

Fig. 6 The overlap of the fluorescence spectra of BSA (a) and the absorbance spectra of the complex (b) at 298.15 K. c(BSA)=c(the complex)=1.0 × 10^{-6} mol L^{-1}.

2.3.4 The effect of the complex on the conformation of BSA. The synchronous fluorescence spectrum is usually applied to analysis the conformation of proteins.[45] When the D-value (Δλ) between excitation wavelength and emission wavelength were stabilized at 15 nm, the synchronous fluorescence only exhibited the fluorescence emission of tyrosine residues. However, the main fluorescent monomer of BSA was the tryptophan residues when Δλ=60 nm. It is apparent from the synchronous spectra (Fig. 7), the maximum emission wavelength moderately shift towards long wave when Δλ= 60 nm, whereas no shift is observed when Δλ is 15 nm. This indicates that tyrosine residue microenvironment has not been affected by binding to the complex, whereas the microenvironment of the tryptophan residue has been changed in the direction of reducing the hydrophobicity of the microenvironment.[46] As there are two tryptophan residues with two distinct environments, where Trp. 134 is located on the surface of BSA, whereas Trp. 212 is located in a hydrophobic fold, we conclude that the complex has more probability to bind to Trp. 212 rather than Trp. 134. Hence, this finding demonstrates that BSA undergoes conformation changes around the tryptophan residues, which eventually can induce loose structure in BSA upon binding to the complex.

3. Conclusions

In conclusion, the structure and biological activity of a new synthetic bismuthoxide Schiff-base complex have been described. The complex showed stronger inhibitory effect on *S. pombe* than the free ligand. The fluorescence analysis revealed that the quenching mechanism of BSA by the complex was a static fluorescence quenching with non-radiation energy transfer happening within single molecule. The change of conformation of BSA showed up as the hydrophobicity around the tryptophan residues decreased.

4. Experimental

4.1 Chemicals and instrumentation

All chemicals of analytical or biological grade were used as received, no further purification was done. *S. pombe* (ACCC 20047) was provided by Agricultural Culture Collection of China. The Edinburgh minimal medium (EMM) culture composition was 3 g K_2HPO_4, 2.2 g Na_2HPO_4, 5 g NH_4Cl, and 20 g glucose per liter (natural pH). The yeast extract medium composition was dissolved by 100 mL distilled water and constant volume to 1000 mL (natural pH). BSA was purchased from the Shanghai Bo'ao Biological Technology Co., Ltd. The buffer Tris had a purity of no less than 99.5% and the samples were dissolved in Tris-HCl buffer solution (5 × 10^{-3} mol L^{-1} Tris/ 5 × 10^{-2} mol L^{-1} NaCl, pH=7.4).

Microcalorimetric experiments were performed on a 3116-2/3239 TAM Air Isothermal calorimeter (Thermometric AB, Sweden), which equipped with eight twin calorimetric channels with one side for the sample and the other for a static reference. The structure and operation of the instrument have been described previously.[47] The fluorescence spectra were obtained on an F-4600 fluorescence spectrophotometer (Hitachi, Tokyo, Japan). FTIR spectra (4000-400 cm^{-1}) were done on a Fourier transform IR spectrometer with a KBr pellet (Avatar360, Nicolet, Madison, USA). ^{1}H NMR and ^{13}C NMR were recorded at 400MHz and 100MHz, respectively, with a Bruker DRX-400 spectrometer using DMSO-d_6 as a solvent. Chemical shifts were given in ppm down field (δ) from Me_4Si (TMS) as an internal standard. An elemental analyzer (Elementar Vario EL CUBE, German) was used to measure the C, H, and N contents of the complex.

4.2 Synthesis of the complex

H_2*vanen* was prepared according to the published literature.[48] In a typical experimental procedure, $Bi(NO_3)_3{\cdot}5H_2O$ (4 × 10^{-4} mol, 0.194 g) and mannitol (4 × 10^{-4} mol, 0.0728g) were ground into a smooth paste in an appropriate mortar.[49,50] To this was added 3 mL deionized water and 5 mL methanol in turn and stirred until dissolution. Subsequently, the mixed solution was slowly added dropwise to a stirred methanol solution (25 mL) of H_2*vanen* (8 × 10^{-4} mol, 0.2624 g) at 45~60 °C for 30 minutes. After two hours of continuously stirring, the product was collected by filtration after concentration by rotary evaporation to a small volume and washed

with dichloromethane. Single crystals were obtained by slow diffusion of diethyl ether into the filtrate for several days. The solid product was identified as $[Bi_9O_8(vanen)_3\ (NO_3)_2\ (CH_3OH)_2\ (H_2O)]\cdot 3NO_3\cdot 5.5H_2O$. Yield: 0.098 g, 62.0%. Spectroscopic data of the complex were given as follows: *IR* (KBr): ν (cm^{-1}): 3421.1 (s, ν_{O-H}), 2918.6 (m, ν_{C-H}), 1635.4 (vs, $\nu_{C=N}$), 1449.8 (vs, $\nu_{C=C}$), 1384.0 (vs, ν_{NO3^-}), 1216.9 (s, ν_{Ph-O}), and 1083.6 (s, ν_{C-O}). ^{1}H NMR (400 MHz, DMSO-d_6): δ 8.49 (s, 2H, CH=N), 7.19 (d, J = 7.8 Hz, 2H, ArH), 7.07 (d, J = 7.8 Hz, 2H, ArH), 6.82 (t, J = 7.9 Hz, 2H, ArH), 4.41 (d, J = 5.8 Hz, 2H, CH_2), 4.00 (d, J = 5.9 Hz, 2H, CH_2), 2.82 (s, 6H, CH_3). ^{13}C NMR (100 MHz, DMSO-d_6): δ 166.9(C=N), 150.8 (C-Ph), 150.7 (C-Ph), 127.2 (C-Ph), 124.2 (C-Ph), 117.9 (C-Ph), 115.6 (C-Ph), 62.2 (C-O), 53.2 (C-C). Elemental analysis for the complex ($Bi_9\ C_{56}O_{43.5}H_{75}N_{17}$), Calc. (Found): C 18.88 (18.97), H 2.12 (2.18), N 6.68 (6.56) %.

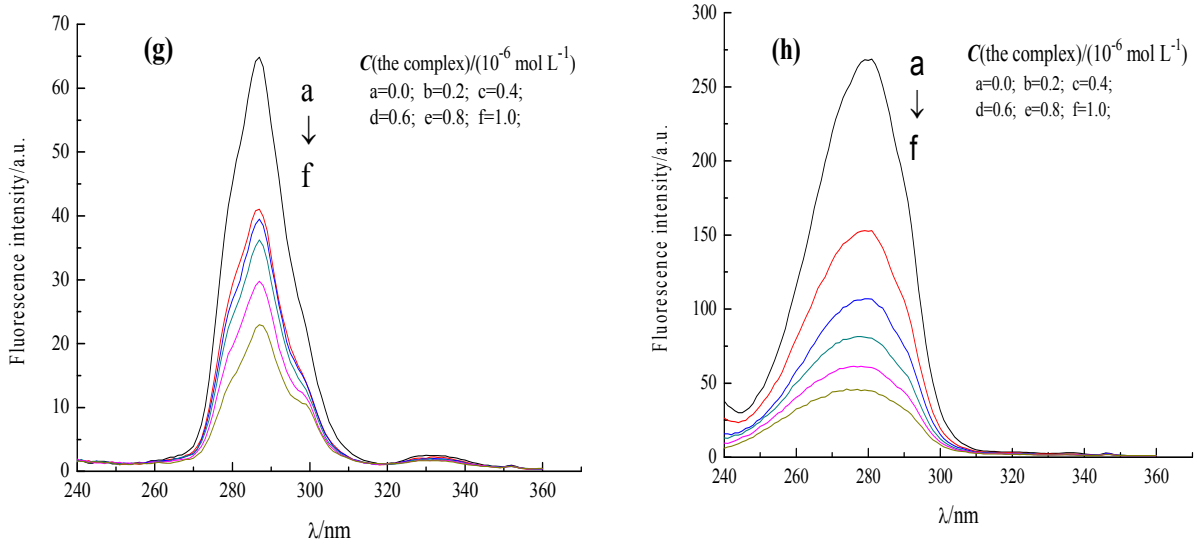

Fig. 7 Synchronous fluorescence spectrum of BSA at 298.15 K. (g) Δλ=15 nm. (h) Δλ=60 nm. *c* (BSA) =1.0 × 10^{-6} mol L^{-1}.

4.3 Solubility and stability

The prepared complex, which is a pale yellow powder, proves to be insoluble in most organic solvents such as ethanol, benzene and diethyl ether, but soluble in DMF and DMSO. It was found that the complex was comparatively stable and could be stored for over one year in air without appreciable degradation. NMR studies showed that, when the complex was kept in deuterated solvent over six months, there was no change in observed NMR shifts of the complex and no evidence of the appearance of any other species, strongly suggesting the complex was very stable in solvent. In general, there is no obvious influence the biological activity of the complex in solvents.

4.4 X-ray crystallographic analysis

Suitable single crystal of the complex was selected for X-ray diffraction analysis. Crystal data was collected on Bruker smart CCD area-detector diffractometer with graphite-monochromated Mo-Ka X-ray radiation (λ= 0.71073 Å) at 173 K and corrected for absorption using the SADABS. Structural solution and refinements were carried out using the SHELX suite of programs with the graphical interface X-Seed. The crystal structure was severely affected by the large heavy-atom content, and therefore data were not as precise as preferred. In the refined process, some restriction was performed with optimal geometries. A few hydrogen atoms were not added in the crystal structure. Crystal data for the complex was shown as follows: $C_{56}\ H_{75}\ Bi_9\ N_{11}\ O_{43.5}$, M_r=3479.07, triclinic, space group *P*–1, a=14.9741(15) Å, b=16.8900(17) Å, c=18.5248(19) Å, α=80.769(2)°, β=84.451(2)°, γ=71.208(2)°, V=4372.89Å^3, Z=2, F(000)=3138.0, ρ_{calcd}=2.63139 g/cm^3, μ=18.135mm^{-1}, $2\theta_{max}$=54.04°, 35927 reflections collected, 14938 unique (R_{int}=0.0403). Final GOF= 1.032, R_1 = 0.0458, wR_2 = 0.1555, R indices based on 11060 reflections with $I > 2\sigma(I)$ (refinement on F^2), R_1 = 0.0686, wR_2 = 0.1555 (all data), 1018 parameters. CCDC 961392 for the complex contains the supplementary crystallographic data for this paper. The data can be obtained free of charge from The Cambridge Crystallographic Data Centre via www.ccdc.Cam.ac.uk/data_request/cif.

4.5 Microcalorimetric measurement

The crystals were applied to assess the biological activity of the complex, which were confirmed to the homogeneity of the crystal yield by PXRD. The microcalorimeter was thermostated at 32 °C, and the measurement made with the ampoule method. Baselines were taken before each measurement and the calorimeter was calibrated electrically. When the system had gained a stable baseline, 5mL EMM-sterilized culture medium was added into the sterilized sample ampoules. *S. pombe* was inoculated with an initial density of 1×10^6 cells mL^{-1}. The samples at different concentrations were added to the cell suspension, respectively. All the ampoules containing the cell suspension of *S. pombe*, were sealed up and put into 8-channel calorimeter block. The data was collected continuously by using the dedicated software package. All the microcalorimetric experiments were repeated three times and the obtained results were identical.

4.6 Fluorescence measurement

All fluorescence spectra were determined on an F-4600 fluorescence spectrophotometer (Hitachi, Japan) equipped with a 1.0 cm quartz cell and a thermostat bath. Excitation wavelength was 280 nm. The widths of both the excitation slit and the emission slit were set to 3.0 nm. Appropriate blanks corresponding to the buffer were subtracted to correct background fluorescence. Fluorescence spectra were recorded in the range of 290 nm and 500 nm at different temperatures (298.15, 302.15, 306.15 and 310.15 K).

Acknowledgements

The authors gratefully acknowledge the financial support of the National Natural Science Foundation of China (Nos. 20973145, 21273190), the Hunan Provincial Key Laboratory Special Foundation of China (Nos. 2014FJ3011, 2014TT2026, 2013FJ3033, 2012XGJSYB02, 2011TP4016-1 and 2012TP4021-5), the Hunan Provincial Educational Ministry Foundation of China (No. 11A112, 15A175, 14A134 and 15C1272), the Hunan Provincial Natural Science Foundation of China (No. 11JJ3019), the Hunan Provincial Colleges and Universities "twelve-five planning" Professional Comprehensive Reform Pilot Project (No. 2012-266), the Construction Project of Hunan Provincial Colleges and Universities Teaching Practice (No. 2013-295), the Scientific Research Foundation of Xiangnan University (Nos. 2013YJ36, 2013YJ37, 2013YJ38), and the Construct Program of the Key Discipline in Hunan Province.

References

1 J. Q. Xie, C. H. Li, J. X. Dong, W. Qu, L. Pan, M. L. Peng, M. A. Xie, X. Tao, C. M. Yu, Y. Zhu, P. H. Zhang, C. G. Tang and Q. G. Li. *Thermochim. Acta*, 2014, **589**, 7.

2 S. Hino, M. Maeda, K. Yamashita, Y. Kataoka, M. Nakano, T. Yamamura, H. Nojiri, M. Kofu, O. Yamamurod and T. Kajiwara, *Dalton Trans*., 2013, **42,** 2683.

3 D. Ghosh, P. K. Bera, M. Kumar, S. H. R. Abdi, N. H. Khan, R. I. Kureshy and H. C. Bajaj, *RSC Adv*., 2014, **4**, 56424.

4 B. Cristovao, J. Klak, R. Pelka, B. Miroslaw and Z. Hnatejko, *Polyhedron*, 2014, **68**, 180.

5 S. Sarkar and S. Mohanta, *RSC Adv*., 2011, **1**, 640.

6 S. Mondal, S. Hazra, S. Sarkar, S. Sasmal and S. Mohanta, *J. Mol. Struct*., 2011, **1004**, 204.

7 P. C. Andrews, R. L. Ferrero, P. C. Junk, I. Kumar, Q. Luu, K. Nguyena and J. W. Taylora, *Dalton Trans*., 2010, **39**, 2861.

8 G. G. Briand and N. Burford, *Chem. Rev*., 1999, **99**, 2601.

9 S. Suerbaum and P. Michetti, *New. Engl. J. Med.*, 2002, **347**, 1175.

10 H. Y. Li and H. Z. Sun, *Curr. Opin. Chem. Biol*., 2012, **16**, 74.

11 Y. Kondo, S. Himeno, M. Satoh, A. Naganuma, T. Nishimura and N. Imura, *Cancer Chemother. Pharmacol*., 2004, **53**, 33.

12 M. X. Li, M. Yang, J. Y. Niu, L. Z. Zhang and S. Q. Xie, *Inorg. Chem*., 2012, **51**, 12521.

13 M. X. Li, Y. L. Lu, M. Yang, Y. K. Li, L. Z. Zhang and S. Q. Xie, *Dalton Trans*., 2012, **41**, 12882.

14 M. X. Li, L. Z. Zhang, M. Yang, J. Y. Niu and J. Zhou, *Bioorg. Med. Chem. Lett*., 2012, **22**, 2418.

15 L. Z. Zhang, G. Y. An, M. Yang, M. X. Li and X. F. Zhu, *Inorg. Chem. Commun*., 2012, **20**, 37.

16 O. Braissant, G. Bonkat, D. Wirz and A. Bachmann, *Thermochim. Acta*, 2013, **555**, 64.

17 Y. W. Wu, W. Y. Gao, X. H. Xiao and Y. Liu, *Thermochim. Acta*, 2005, **429**, 167.

18 W. J. Kong, Y. L. Zhao, X. Y. Xing, X. P. Ma, X. J. Sun, M. H. Yang and X. H. Xiao, *Appl. Microbiol. Biotechnol*, 2015, **99**, 6049.

19 O. Braissant, A. Bachmann and G. Bonkat, *Methods*, 2015, **76**, 27.

20 H. N. Hou, J. C. Zhu, Y. Liu and Q. G. Li, *Acta Phys. -Chim. Sin*., 2007, **23**, 987.

21 G. Vignesh, K. Sugumar, S. Arunachalam, S. Vignesh and R. Arthur James, *Spectrochim. Acta Part A*, 2013, **113**, 415.

22 Y. Jung and S. J. Lippard, *Chem. Rev*., 2007, **107**, 1387.

23 A. Bergamo and G. Sava, *Dalton Trans*., 2007, **13**, 1267.

24 T. Peter, *Adv. Protein Chem*., 1985, **37**, 161.

25 Y. Moriyama, D. Ohta, K. Hachiya, Y. Mitsui and K. Takeda, *J. Protein Chem*., 1996, **15**, 265.

26 B. K. Paul, A. Samanta and N. Guchhait, *J. Phys. Chem. B*, 2010, **114**, 6283.

27 C. H. Li, J. H. Jiang, P. Yang, L. M. Tao, X. Li, S. X. Xiao, X. Tao, J. Q. Xie, Y. Zhu, and Q. G. Li, *J. Therm. Anal. Calorim*., 2015, **119**, 1285.

28 J. Q. Xie, C. H. Li, J. X. Dong, W. Qu, L. Pan, M. L. Peng, M. A. Xie, X. Tao, C. M. Yu, Y. Zhu, P. H. Zhang, C. G. Tang and Q. G. Li, *Thermochim. Acta*, 2014, **589**, 7.

29 C. H. Li, X. Z. Song, J. H. Jiang, H. W. Gu, L. M. Tao, P. Yang, X. Li, S. X. Xiao, F. H. Yao, W. Q. Liu, J. Q. Xie, M. N. Peng, L. Pan, X. B. Wu, C. Jiang, S. Wang, M. F. Xu and Q. G. Li, *Thermochim. Acta*, 2014, **581**, 118.

30 C. H. Li, L. M. Tao, S. X. Xiao, A. T. Li, J. H. Jiang, X. Li, F. H. Yao, W. P. Luo, J. Q. Xie, M. N. Peng, L. Pan and Q. G. Li, *Thermochim. Acta*, 2013, **569,** 97.

31 J. C. Cortes, E. Carnero, J. Ishiguro, Y. Sanchez, A. Durán and J. C. Ribas, *J. Cell. Sci*., 2005, **118**, 157.

32 A. Ruiz–Martinez, D. Casanova and S. Alvarez, *Dalton Trans.*, 2008, 2583.

33 C. L. Xie, H. K. Tang and S. S. Qu, *Thermochim. Acta*, 1988, **123**, 33.

34 H. X. Zhang, X. Huang, P. Mei, K. H. Li and C. N. Yan, *J. Fluoresc*., 2006, **16**, 287.

35 A. Sułkowska, *J. Mol. Struct*., 2002, **614**, 227.

36 J. R. Lakowicz, *Principles of Fluorescence Spectroscopy*, second ed., Plenum Press, New York, 1999.

37 W. R. Ware, *J. Phys. Chem*., 1962, **66**, 455.

38 G. Valensin, T. Kushnir and G. Navon, *J. Magn. Reson*., 1982, **46**, 23.

39 M. Jiang, M. X. Xie, D. Zheng, Y. Liu, X. Y. Li and X. Chen, *J. Mol. Struct*., 2004, **629**, 71.

40 Y. V. llichev, J. L. Perry and J. D. Simon, *J. Phys. Chem. B*., 2002, **106**, 452.

41 L. Cyril, J. K. Earl and W. M. Sperry, *Biochemists' Handbook*, E. & F. N. Spon, London, 1961, pp. 84.

42 S. Weiss, Science, 1999, **283**, 1676.

43 B. Valeur, J. C. Brochon, *New Trends in Fluorescence Spectroscopy*, Springer, Berlin, 2001, pp. 25.

44 B. Valeur, *Molecular Fluorescence: Principles and Applications*, Wiley Press, New York, 2001, pp. 250.

45 J. N. Miller, *Anal. Proc.*, 1979, **16**, 203.
46 K. H. Ulrich, *Pharmacol. Rev.*, 1981, **33**, 17.
47 X. Li, J. H. Jiang, Q. Q. Chen, S. X. Xiao, C. H. Li, H. W. Gu, H. Zhang, J. L. Hu, F. H. Yao and Q. G. Li, *Eur. J. Med. Chem.*, 2013, **62**, 605.
48 T. Gao, P. F. Yan, G. M. Li, G. F. Hou and J. S. Gao, *Inorg. Chim. Acta*, 2008, **361**, 2051.
49 H. D. Yin, C. H. Wang and Q. J. Xing, *Chin. J. Chem.*, 2005, **23**, 1631.
50 H. D. Yin, S. C. Xue and C. H. Wang, *Chinese J. Struct. Chem.*, 2004, 23, 1356.

